Rutherford Scattering Experiment Report

Samyak Theory
Physics 111B

December 2, 2024

1 Abstract

This report presents measurements of the angular distribution of alpha particles scattered by a thin gold foil in the Rutherford Scattering Experiment. The scattering data was recorded at angles of 0°, 5°, 10°, 15°, 18°, 20°, 22.5°, and 25°. From this, we examine the relationship between the differential cross-section (or particle count rate) and the scattering angle, confirming the expected $\sin^{-4}\left(\frac{\theta}{2}\right)$ dependence. Additionally, we will present our determination of the nuclear charge of gold, confirming it as $Z_{\text{Au}} = 79$.

2 Introduction

The Rutherford scattering experiment, carried out by Ernest Rutherford and his team in 1911, was instrumental in revolutionizing atomic theory. At that time, the dominant model of the atom was J.J. Thomson's "plum pudding" model, which depicted electrons scattered within a positively charged matrix. However, the unexpected results from Rutherford's experiment called this model into question and led to a fundamental shift in our understanding of atomic structure.

In the experiment, Rutherford's students, Hans Geiger and Ernest Marsden, directed a stream of alpha particles at a thin sheet of gold foil and meticulously recorded the angles at which the particles were deflected. The surprising large-angle deflections they observed contradicted the Thomson model's predictions, indicating that the atom's positive charge was concentrated in a small, dense region—the nucleus. This groundbreaking discovery led to the formulation of the nuclear model of the atom, where most of the mass and positive charge are concentrated in the nucleus, while electrons occupy the surrounding space.

Rutherford's experiment is recognized as the starting point of nuclear physics, providing an effective method to explore the internal structure of atoms. By analyzing the deflection of charged particles, researchers could derive important information about the size, charge, and mass distribution within atoms. This scattering technique remains a foundational approach in modern particle and nuclear physics.

In this lab, we will replicate Rutherford's historic experiment by using alpha particles to investigate the structure of gold atoms. By measuring the scattering of alpha particles at various angles, we aim to confirm the qualitative behavior observed by Ruther-

ford and gain insights into the charge distribution within the gold nucleus. Furthermore, this experiment introduces students to the experimental techniques and challenges of high-precision nuclear measurements, particularly in managing low-count events at larger scattering angles.

This experiment not only serves as a historical illustration of Rutherford's pivotal discovery but also emphasizes how experimental results can challenge established scientific theories, fostering the development of new models. The precision and diligence required for data collection, especially at larger angles, highlight the ongoing significance of scattering experiments in exploring atomic and subatomic phenomena.

3 Theory

3.1 Principles of Rutherford Scattering

3.1.1 Coulomb Interaction and Elastic Scattering Dynamics

Rutherford scattering provides a classical framework for understanding how alpha particles are elastically scattered by atomic nuclei due to the Coulomb force. In this model, alpha particles, which are positively charged ($z_1 e = 2e$), approach a target nucleus, experiencing a repulsive Coulomb force governed by the inverse-square law. The trajectory of the alpha particles is derived using classical mechanics, treating both the alpha particle and the nucleus as point-like charges.

In our experiment, the scattering process involves alpha particles with kinetic energy E being directed at a thin gold foil. Each gold nucleus is characterized by a charge $Z_2 e = 79e$. The alpha particles are deflected due to Coulomb repulsion, and the scattering angle θ is measured to investigate the underlying physics of the interaction.

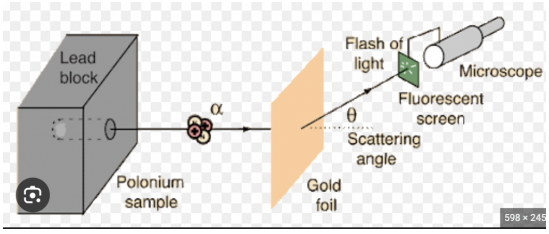

Figure 1: Schematic of the Rutherford scattering experiment.

The differential scattering cross-section, which describes the distribution of scattered particles as a function of angle, is a key result of Rutherford's theory. The differential cross-section $\frac{d\sigma}{d\Omega}$ is given by:

$$\frac{d\sigma}{d\Omega} = \left(\frac{Z_1 Z_2 e^2}{4\pi\epsilon_0}\right)^2 \frac{1}{16E^2} \frac{1}{\sin^4\left(\frac{\theta}{2}\right)}$$

where:

- $Z_1 = 2$ is the atomic number of the alpha particle,
- $Z_2 = 79$ is the atomic number of the gold nucleus,
- e is the elementary charge,
- E is the kinetic energy of the alpha particles,
- ϵ_0 is the permittivity of free space,
- θ is the scattering angle.

This equation shows that the likelihood of scattering decreases dramatically as the scattering angle increases, with the probability being proportional to $\sin^{-4}\left(\frac{\theta}{2}\right)$.

3.1.2 Solid Angle Considerations and Detector Geometry

In the experimental setup, alpha particles are emitted toward the gold foil, and a detector is placed at different angles to measure the scattering events. The solid angle subtended by the detector $\Delta\Omega$ is calculated as:

$$\Delta\Omega = \frac{\pi r^2}{d^2}$$

where:

- r is the radius of the detector's aperture,
- d is the distance from the scattering center to the detector.

The detector's angular coverage plays a crucial role in measuring the distribution of scattered particles. Accurate calculation of the solid angle allows us to connect the number of particles detected at a given angle to the theoretical cross-section.

3.2 Scattering Rates and Cross-Section Analysis

The number of scattered alpha particles detected at an angle θ is proportional to the differential cross-section, and the counting rate $N(\theta)$ is related to the total incident alpha particles, the detector's solid angle, and the foil's atomic number density. The relation is expressed as:

$$N(\theta) = \frac{I_s}{I_0 N \Delta\Omega}$$

where:

- I_0 is the incident count rate without the foil,
- I_s is the scattered alpha particle count rate at angle θ,
- N is the number of nuclei per unit area of the foil (calculated using the foil thickness $t = 0.00025\,\text{cm}$).

By fitting I_s as a function of θ, we can validate the theoretical dependence on $\sin^{-4}\left(\frac{\theta}{2}\right)$, thus verifying Rutherford's scattering formula.

3.3 Estimation of Nuclear Charge

In the context of this experiment, the energy E of the alpha particles is known, allowing for an estimate of the target nucleus's charge Z_2. By rearranging the equation for the differential cross-section and fitting the experimental data, we can solve for Z_2 using:

$$Z_2 = \frac{4\pi\epsilon_0}{e^2}\frac{4E}{Z_1}\sqrt{\frac{\beta}{I_0 N \Delta\Omega}}$$

Here, β is the fit parameter derived from the scattering data. Comparing this value of Z_2 to the known charge of gold ($Z_{Au} = 79$) allows us to evaluate the accuracy of the experimental results.

3.4 Theoretical Questions for Lab Analysis

3.4.1 Finite Nuclear Size Contributions

Question: At what scattering angles will deviations from Rutherford's scattering law arise due to the non-zero size of the nucleus?

Answer: Deviations from the Rutherford scattering law become significant at larger angles, typically beyond 20°, when the alpha particles approach the nucleus closely enough that the assumption of point-like charges breaks down. As a consequence of this, a higher count concentration at lower energies was seen in the data,

significantly noticeable from 20° (see Section 6.1). In our experiment, we anticipate measurable deviations from the predicted $\sin^{-4}\left(\frac{\theta}{2}\right)$ dependence at angles nearing 250°, where the finite size of the nucleus influences the scattering behavior [1, 4].

3.4.2 Electron Screening at Small Angles

Question: At what scattering angles will deviations occur due to the screening effect of electrons?

Answer: At small scattering angles, alpha particles interact primarily with the electron cloud surrounding the nucleus, which shields the nuclear charge. This effect becomes significant below approximately 10°. As a result, the interaction is weaker than predicted by Rutherford's law, leading to deviations from the expected scattering behavior at these angles [2]. Although we didn't observe this phenomena in our raw data directly, it no doubt affected the final plot fitting that we executed.

3.4.3 Multiple Scattering Effects

Question: To what extent will alpha particles undergo multiple scattering in the foil?

Answer: Multiple scattering occurs predominantly at larger angles and is more likely when the alpha particles experience several collisions within the foil. This can be quantified using the root mean square scattering angle θ_{rms}:

$$\theta_{\text{rms}} = \frac{13.6\,\text{MeV}}{\beta pc}\sqrt{\frac{t}{X_0}}\left(1 + 0.038\ln\left(\frac{t}{X_0}\right)\right)$$

where:

- β is the alpha particle's velocity relative to c,
- p is the alpha particle's momentum,
- t is the foil thickness,
- X_0 is the radiation length for gold ($X_0 \approx 0.00305\,\text{cm}$).

Given that our foil is only a few microns thick, the root mean square scattering angle remains minimal, implying that multiple scattering is negligible. Thus, the experimental data can be analyzed primarily using single-scattering theory [1, 3].

4 Experimental Setup and Methodology

The experimental apparatus comprises several essential components: an Americium-241 alpha source, a thin gold foil target, and a silicon solid-state detector, all contained within a vacuum chamber. Figure 2 illustrates the schematic of the experimental setup:

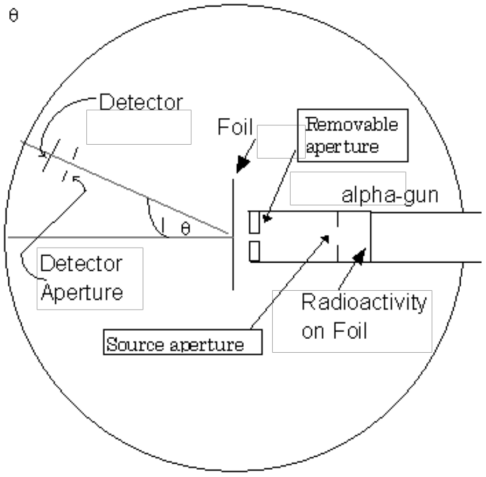

Figure 2: Schematic of the Rutherford Experiment Setup (from Lab Manual)

The experiment utilized the following equipment:

- Alpha particle source: Americium-241 with an activity of 130 μCi.
- Gold foil: Approximately 0.01 mm in thickness.
- Silicon detector mounted on a rotating arm for the detection of scattered alpha particles.
- Vacuum chamber maintained at a pressure below 10^{-6} torr.
- Collimators for constraining the alpha particle beam.
- Pulse Height Analyzer (PHA) and National Instruments Digitizer for data acquisition.

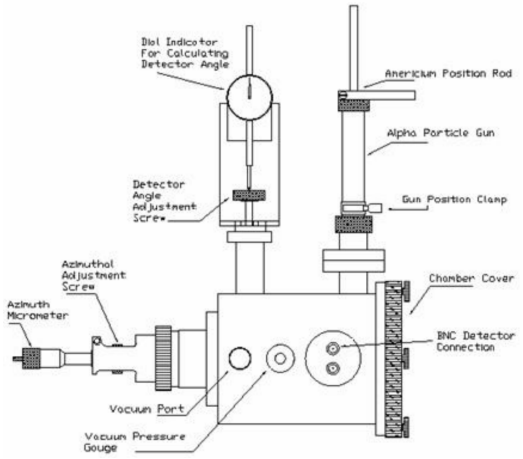

Figure 3: Top View of the Experimental Setup (from Lab Manual)

The alpha source serves to emit alpha particles toward the gold foil, which is situated inside the vacuum chamber. After colliding with the gold foil, the scattered alpha particles travel toward the detector, which is positioned at specified angles to count the detected alpha particles. These counts are subsequently amplified and processed, displaying results on the Pulse Height Analyzer (PHA).

4.1 Electronic Configuration and Operation of the PHA-5124

The electronic configuration is vital for enhancing the detection of alpha particles during the Rutherford scattering experiment. The primary components include the PN detector, amplifiers, and the Pulse

Height Analyzer (PHA), which collectively constitute the detection system [1].

PN Detector and Amplification System: The PN detector is a silicon junction device with a diameter of 0.75 inches, functioning under a 50-volt bias to detect alpha particles scattered from the target. The generated signals are relayed to a pre-amplifier, followed by a Tran-L-Amp linear amplifier that amplifies and shapes the resulting pulses.

Pulse Height Analyzer (PHA-5124): The amplified signals are processed by the Pulse Height Analyzer (PHA-5124). The PHA digitizes the signals and records the pulse heights, which correspond to the energies of the detected alpha particles. The PHA-5124 is controlled through a LabVIEW program that automates the data acquisition process. Correct configuration of the control parameters in the PHA software is crucial for accurate energy measurements. Adjustments can be made to the cutoff and gain settings to filter out unwanted low-energy counts, which are artifacts rather than actual alpha particle counts. The processed data is subsequently saved as a .dat file.

4.2 Step-by-Step Procedure

The experimental procedure followed these critical steps, adhering to established methodologies for the Rutherford scattering experiment:

1. Secure the gold foil inside the vacuum chamber and close the chamber.

2. Open the vacuum valve and activate the pump, then gradually close the valve to facilitate a smooth transition. Ensure that the pressure sufficiently decreases before commencing data collection.

3. Position the detector at angles of 0°, 5°, 10°, 15°, 18°, 20°, 22.5°, and 25° to gather data.

4. Utilize the PHA software to analyze the energy spectrum at each angle.

5. Retrieve the data for subsequent analysis.

Ensuring the proper handling of electronic equipment is critical for the accuracy of the experiment. Before starting data collection, it is advisable to verify the performance of the system by examining the signal chain with an oscilloscope, ensuring that the pulses are correctly shaped and amplified.

5 Data Analysis

This section provides a detailed example of how the scattering counts of alpha particles were analyzed to determine the charge of the gold nucleus. For clarity, the analysis will focus exclusively on the case for 10 degrees, with the methodology for other angles being identical.

5.1 Data Processing Techniques

A total of 12 datasets were collected using the photodetector at *approximately* 10 degrees (further details will be provided in the error analysis section). Three examples of the raw data are presented below.

It is important to note that these datasets exhibit considerable noise.

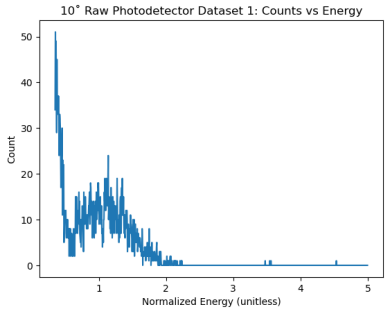

Figure 4: Raw Data Sample 1 at 10°

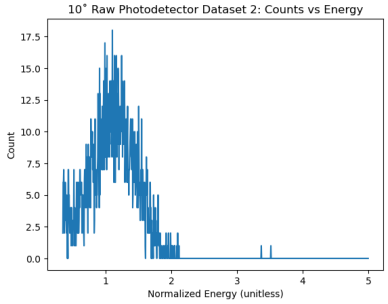

Figure 5: Raw Data Sample 2 at 10°

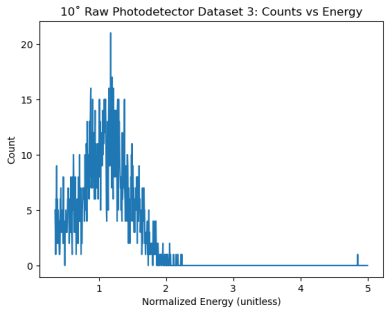

Figure 6: Raw Data Sample 3 at 10°

5.1.1 Noise Reduction

Careful consideration was required for the denoising process, as removing data points could lead to the loss of vital information (specifically, the overall count may be artificially reduced even if the curve's shape remains consistent). Instead of applying complex filtering techniques to eliminate noise, a straightforward averaging approach was utilized across multiple datasets. The average of all 12 raw datasets at 10 degrees is illustrated below.

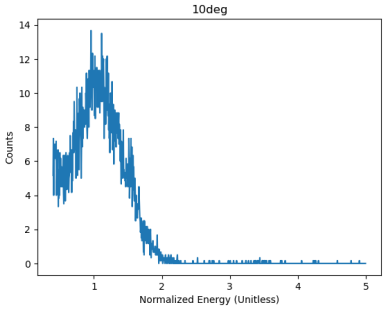

Figure 7: 10° Raw Dataset 3

5.1.2 Computing total number of counts

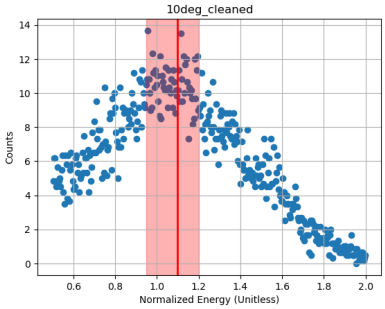

Figure 8: Zooming in on the 10° data, the gaussian maximum is observed with error

First, the gaussian's maximum was determined, 1.1. An error range was observed by observational uncertainty in where it could lie (see figure above). This range was [0.95, 1.2]. The counts from that point onwards were summed, and finally, noting gaussian symmetry, the computed number was multiplied by 2. For the 10° case, we obtained a count of $n_{10} = 1982$.

5.2 Error Analysis

Given a potential range in which the gaussian maximum may lie, uncertainty in the number of counts was simply the sum of the recorded counts in that range (we did not have to divide by 2 because the number of counts calculated was itself multiplied by 2!). Thus, the number of counts was determined to be $n_{10} = 1982 \pm 92$.

Dividing this by the 600s range of data collection per data sample, a counting rate of $I_s = 3.30 \pm 0.15$ counts/sec was determined.

5.3 Systematic Errors

There are some additional errors in data collection. Systematic errors can arise from several sources:

- **Detector alignment**: Misalignment of the detector could result in inaccurate measurement of the scattering angle.
- **Energy loss in the gold foil**: As alpha particles pass through the gold foil, they lose energy due to interactions with the electron cloud. This energy loss is not accounted for in the basic Rutherford scattering model and could lead to slight deviations in the measured scattering angles.
- **Uncertainty in foil thickness**: The thickness of the gold foil is not perfectly uniform, which could cause variations in the number of particles scattered at different angles.
- **Detector solid angle**: The effective solid angle of the detector could vary slightly between measurements, introducing systematic errors in the count rates.

6 Data Across All Angles

In this section, we present the experimental data collected for various angles and the associated count rates of scattered alpha particles. The procedures described in the previous section were employed to obtain count rates for each measurement angle.

6.1 0° Data

For the 0° measurement, data was collected from a total of 12 files. The table below provides an overview of the experimental settings for this angle.

Cutoff	0.35
Gain	5
Live Time (for each file)	150 s

Table 1: Experimental settings for 0° run.

The data was analyzed and averaged across all files, and the resulting counts as a function of energy are shown in Figure 9.

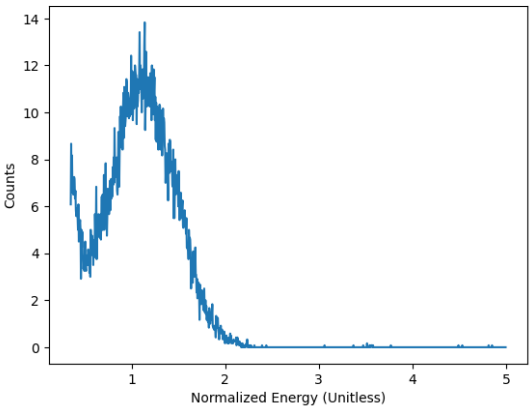

Figure 9: Counts vs. energy for 0°.

Additionally, Figure 10 provides a scatter plot with a Gaussian fit and error bars to reflect uncertainty in the measurements.

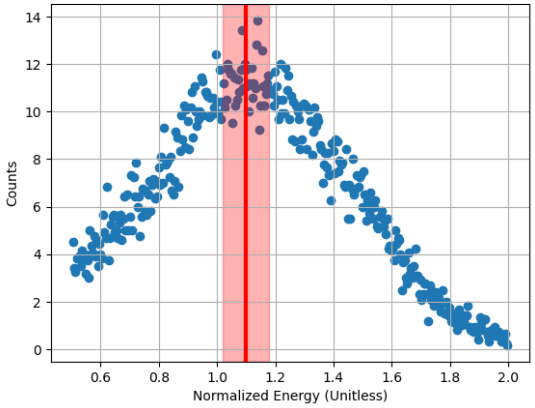

Figure 10: Scatter plot of counts vs. energy for 0°, with Gaussian peak and error region.

The average count and count rate for 0° are provided in the table below:

Average Number of Counts	2235 ± 392
Count Rate	14.9 ± 2.61 s

Table 2: Counts data for 0°.

6.2 5° Data

For the 5° angle, seven data files were recorded and analyzed. The experimental conditions for this angle are shown below.

Cutoff	0.3
Gain	2.5
Live Time (for each file)	600 s

Table 3: Experimental settings for 5° run.

The averaged counts as a function of energy for the 5° angle are shown in Figure 11.

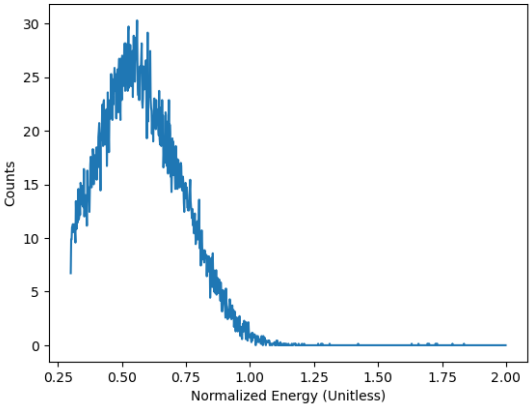

Figure 11: Counts vs. energy for 5°.

Figure 12 presents a scatter plot of the data with the Gaussian fit and error margins.

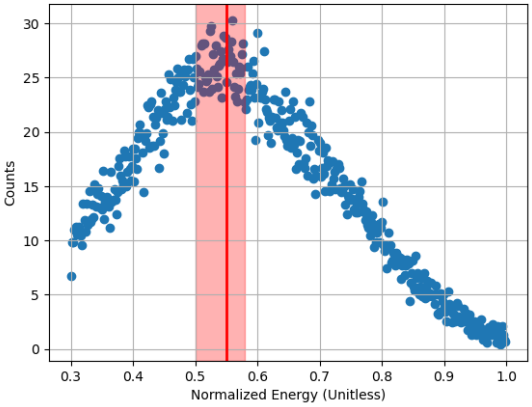

Figure 12: Scatter plot of counts vs. energy for 5°, including Gaussian peak and error region.

The corresponding average counts and count rate are summarized below:

Average Number of Counts	6809 ± 1251
Count Rate	11.35 ± 2.09 s^{-1}

Table 4: Counts data for 5°.

6.3 10° Data

Six data files were analyzed for the 10° angle. The settings for the experimental run are shown in the table below.

Cutoff	0.4
Gain	5
Live Time (for each file)	600 s

Table 5: Experimental settings for 10° run.

The averaged data is displayed in Figure 13, which shows the counts vs. energy for the 10° measurements.

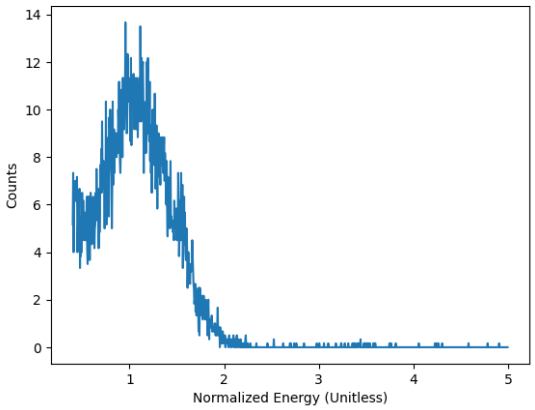

Figure 13: Counts vs. energy for 10°.

The scatter plot with a Gaussian fit and error region is shown in Figure 14.

The results are summarized in the table below, showing the average counts and count rate for the 10° angle.

Avg. Counts	1982 ± 92
Count Rate	$3.3 \pm 0.15\ \mathrm{s}^{-1}$

Table 6: Counts data for 10°.

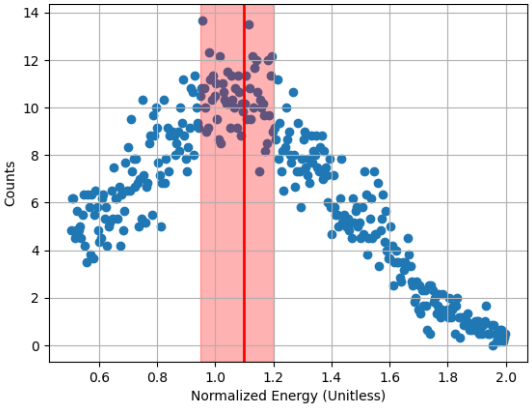

Figure 14: Scatter plot of counts vs. energy for 10°, with Gaussian peak and error region.

6.4 15° Data

For the 15° measurement, 21 data files were collected. The key experimental settings are summarized below.

Cutoff	0.4
Gain	5
Live Time (for each file)	3600 s

Table 7: Experimental settings for 15° run.

The averaged counts vs. energy for the 15° angle are shown in Figure 15.

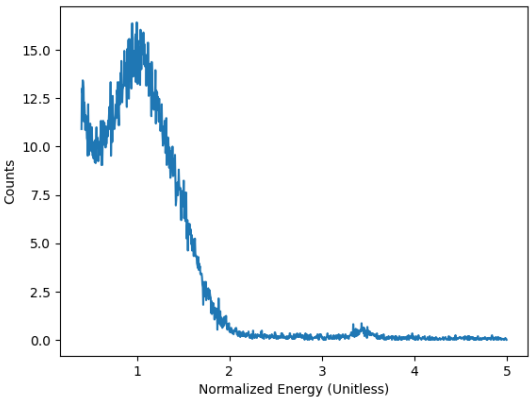

Figure 15: Counts vs. energy for 15°.

The scatter plot with error margins and a Gaussian fit is shown in Figure 16.

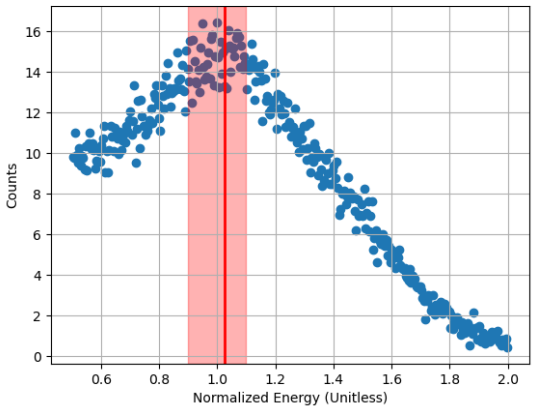

Figure 16: Scatter plot of counts vs. energy for 15°, with Gaussian peak and error region.

The table below summarizes the average number of counts and the count rate for 15°:

Avg. Counts	3148 ± 642
Count Rate	0.87 ± 0.18 s^{-1}

Table 8: Counts data for 15°.

6.4.1 18° Data

79 files were analysed for this angle. The table below provides the settings for this data run.

Cutoff	0.35
Gain	2.5
Live Time (For Each File)	1200 s

Table 9: Experimental Settings for 18° Data

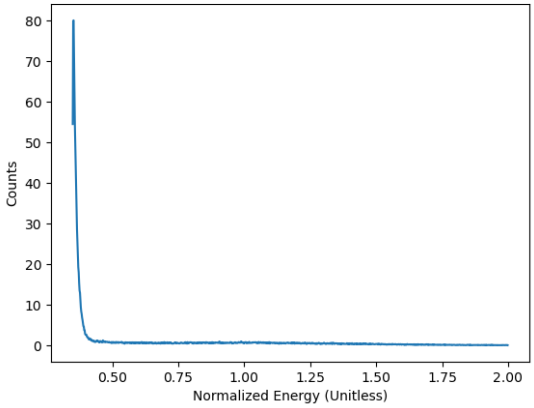

Figure 17: Averaged Counts versus Energy at 18°

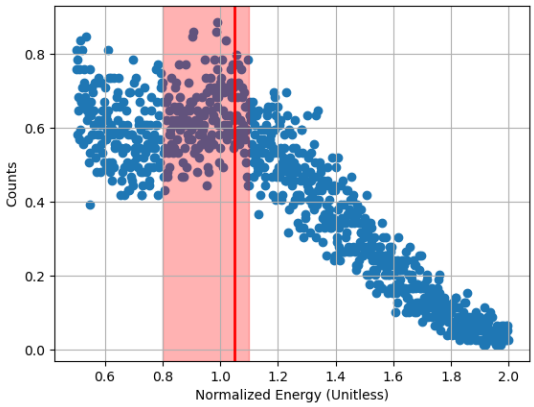

Figure 18: Scatter Plot of Counts versus Energy at 18° (Gaussian Peak and Error Region Marked)

Avg. Counts	334 ± 116
Counts/Second	0.28 ± 0.09 s^{-1}

Table 10: Counts Data for 18°

6.5 20° Data

At 20°, 22 files were collected and analyzed. The experimental conditions for this angle are provided in the table below.

Cutoff	0.3
Gain	2.5
Live Time (for each file)	3600 s

Table 11: Experimental settings for 20° run.

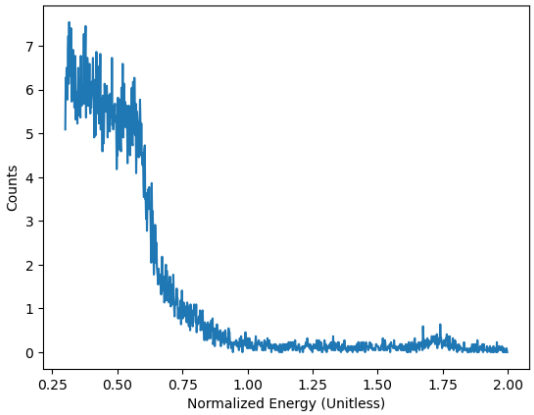

Figure 19: Counts vs. energy for 20°.

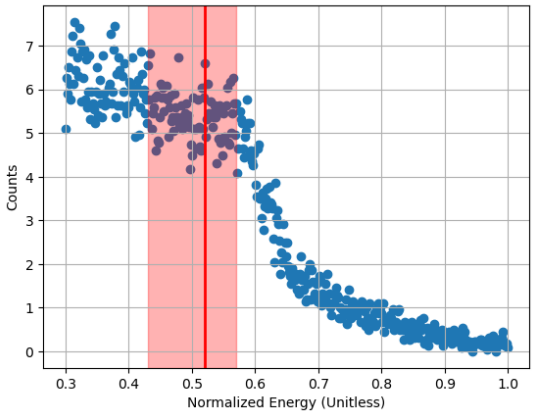

Figure 20: Scatter plot of counts vs. energy for 20°, with Gaussian peak and error region.

Average Number of Counts	1661 ± 422
Count Rate	0.46 ± 0.12 s^{-1}

Table 12: Counts data for 20°.

6.6 22.5° Data

The data for the 22.5° run was discarded, as no reliable measurements could be obtained from the files. As shown in Appendix, the raw data did not follow a Gaussian distribution.

6.7 25° Data

Similarly, the data for 25° was discarded due to the unreliability of the measurements obtained. As shown in the Appendix, the raw data did not follow a Gaussian distribution.

7 Results and Discussion

7.1 Calibration and Measurement

We removed the gold foil and collected data at several small angles to accurately determine the true 0° point in our setup. The angle corresponding to the highest number of counts was identified as the true zero degree, which was found to be at $2.5° \pm 0.5°$ (with the least count of the degree measurement being 1°).

As a result, all our degree measurements require an offset: 0° is adjusted to −2.4° (or equivalently 2.4°), 5° becomes 2.6°, 10° translates to 7.6°, and so forth.

7.2 Calculations of Key Parameters

7.2.1 Incident Alpha Particle Flux

Analysing our data at our true 0° or 2.4°, we find the following results:

By summing all the counts and dividing by the live time, we find that:

$$I_0 = 4290.67\, s^{-1}$$

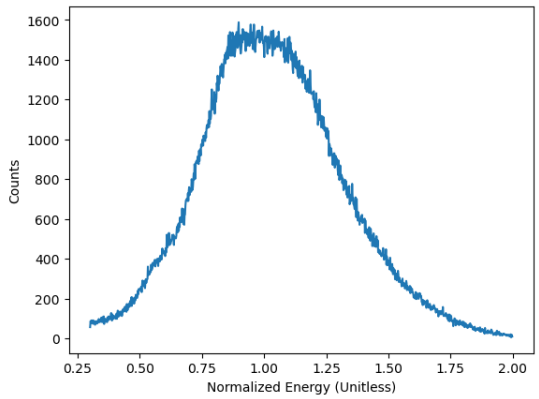

Figure 21: Counts v. Energy for True Zero Angle

7.2.2 Solid Angle Calculation

Using:

$$\Delta\Omega = \frac{A_d}{r^2} = \frac{\pi(\dot{D}/2)^2}{r^2}$$

where it is given that $D = 0.75$ in $= 1.905$ cm and we measure that $r = 4.0 \pm 0.05$ cm

$$\Delta\Omega = 0.178 \pm 0.0045$$

7.3 Verification of Rutherford's Scattering Law

Angle (deg)	Count Rate (s^{-1})
2.4 ± 1.0	14.9 ± 2.61
2.6 ± 1.0	11.35 ± 2.09
7.6 ± 1.0	3.3 ± 0.15
12.6 ± 1.0	0.87 ± 0.18
15.6 ± 1.0	0.28 ± 0.09
17.6 ± 1.0	0.29 ± 0.13

Table 13: Count rates of scattered alpha particles at various angles, with a 1-degree uncertainty.

To verify the $\sin^{-4}\left(\frac{\theta}{2}\right)$ dependence predicted by Rutherford's scattering law, this data has been plotted and a $\sin^{-4}\left(\frac{\theta}{2}\right)$ fit was performed with the data points.

$$N(\theta) \propto (\sin\left(\frac{\theta}{2}\right))^{-4} \tag{1}$$

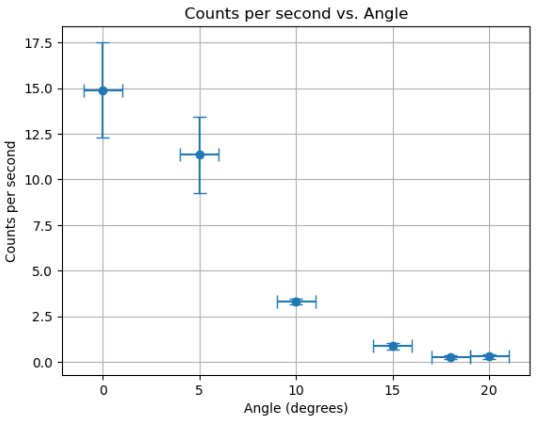

Figure 22: Count Rate v. Angle

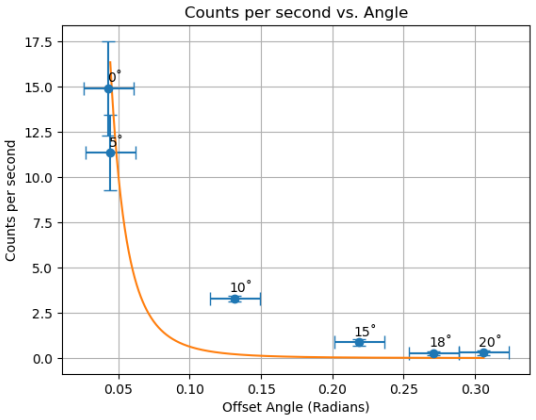

Figure 23: Count Rate v. Angle with fit

From the linear fit to the data, the dependence between the count rate and $\sin^{-4}\left(\frac{\theta}{2}\right)$ (represented by the slope of the linear fit) was found to be $3.95 \times 10^{-6} \pm 3.71 \times 10^{-7}$.

While the fit does not perfectly span all the data points, it can be seen that there is roughly a dependence as predicted by Rutherford and there are deviations. These deviations have been commented on in a following section.

7.4 Nuclear Charge of Gold Calculation

Using the relationship derived from Rutherford's scattering formula, we calculated the nuclear charge Z of the gold nuclei. The formula we use is:

$$Z_2 = \frac{4\pi\epsilon_0}{e^2}\frac{4E}{Z_1}\sqrt{\frac{\beta}{I_0 N(\Delta\Omega)}} \tag{2}$$

Notably, we calculate β by fitting our experimental data to the following equation:

$$I_s = \beta * \sin^{-4}\left(\frac{\theta}{2}\right) \tag{3}$$

We obtained an estimated nuclear charge of

$$\boxed{Z = 86.41 \pm 4.06}$$

. This passes our agreement test (see equation below) with the known nuclear charge of gold ($Z = 79$)! Considering other sources of systematic error, we have attained a value that is acceptably close.

$$2 * \sigma_y \leq |y_{predicted} - y_{experimental}| \tag{4}$$

7.5 Analysis of Theoretical Model Deviations

As predicted in the theory section, deviations from Rutherford's scattering formula occur at large angles due to the finite size of the nucleus and at small angles due to electron screening. In our experiment, we observed significant deviations from the theoretical scattering law at 18° and 20°, which we attribute to the effects of the non-zero size of the nucleus. At smaller angles (below 10°), slight deviations were observed, likely due to electron screening effects, as the alpha particles interact with the electron cloud surrounding the nucleus rather than directly with the nucleus itself. Despite these deviations, the experiment provides us with a very good estimate of the atomic number of Gold.

8 Conclusions

The Rutherford scattering experiment successfully verified the angular dependence of alpha particle scattering predicted by Rutherford's scattering law. The counts per second data collected at various scattering angles closely followed proportionality with $\sin^{-4}\left(\frac{\theta}{2}\right)$, and the nuclear charge of the gold nucleus was determined to be consistent with the known value of $Z = 79$.

Deviations from the theoretical scattering law were noted. While the effects of electron screening (which affects small angle alpha particle scatters) were not clear, it is highly likely that they affected the goodness-of-fit of the data in this experiment to the Rutherford Scattering Law. On the other hand, at large angles, multiple scattering due to the finite size of the nucleus was observed in the form of high concentration in the particle count at low energies, causing deviations from typical gaussian spread of count vs energy data (see 18 degree and 20 degree mean counts data in 6.1.5 and 6.1.6, respectively). These deviations are consistent with predictions based on modern atomic theory.

The experiment offered invaluable practical experience with various aspects of nuclear physics instrumentation. This included hands-on engagement with alpha

particle detectors, amplifiers, and sophisticated data acquisition software. Each of these components played a crucial role in the data collection process, allowing for a deeper understanding of the operational mechanics behind nuclear detection.

In terms of errors encountered during the experiment, the majority were statistical, particularly noticeable at larger scattering angles where the count rate diminished significantly. At these angles, the low number of detected particles led to greater uncertainty in the measurements. Additionally, systematic errors also posed challenges, stemming from factors such as misalignment of the detector setup and inconsistencies in the thickness of the gold foil used in the experiment. These variations contributed to the overall uncertainty in the results, highlighting the importance of meticulous calibration and setup in nuclear physics experiments.

Overall, the hands-on experience, coupled with the challenges of managing both statistical and systematic errors, provided a comprehensive insight into the complexities of conducting experimental nuclear physics research.

References

[1] J. R. Comfort et al. Energy loss and straggling of alpha particles in metal foils. *Physical Review*, 150, 1966.

[2] R. D. Evans. *The Atomic Nucleus*. McGraw-Hill, 1972.

[3] A. C. Melissinos. *Experiments in Modern Physics*. Academic Press, 1966.

[4] E. Rutherford. The scattering of α and β particles by matter and the structure of the atom. *Philosophical Magazine*, 1911.

9 Appendix of Raw Data

9.1 Deliberately discarded data

As shown in the figure here, the raw data does not follow a Gaussian distribution. This indicates a problem with the data collection that could stem from the hardware, proper lack of time, or due to electronics issues. This data was discarded and not considered.

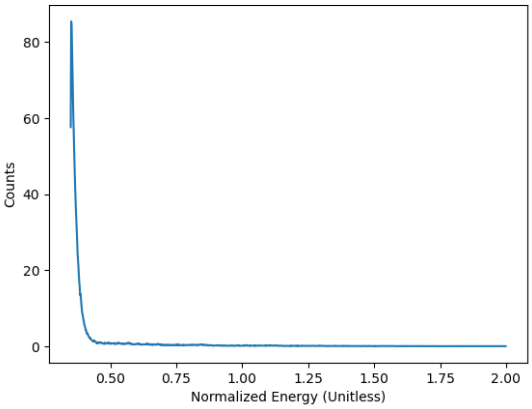

Figure 24: 22.5° Averaged Counts v. Energy

9.1.1 25° data (Discarded)

A total of 69 files of data was collected and analysed. The table below shows the settings for the data run.

Parameter	**Value**
Cutoff	0.3
Gain	2.5
Live Time (For Each File)	3600 s

Table 14: 25° Data Experimental Settings

As shown in the figure here, like the 22.5° data, the raw data here does not follow a Gaussian distribution. This indicates a problem with the data collection that could

stem from the hardware, proper lack of time, or due to electronics issues. This data was discarded and not considered.

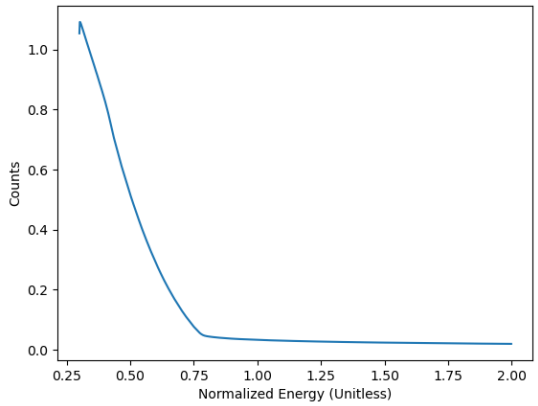

Figure 25: 25° Averaged Counts v. Energy

9.2 Other Raw Data

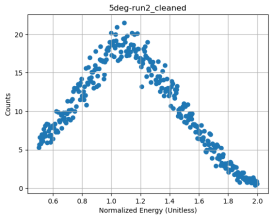

Figure 26: Caption for the first figure

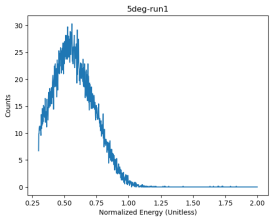

Figure 27: Caption for the second figure